NASA Technical Paper 1655

Velocity-Split Navier-Stokes Solution Procedure for Incompressible High Reynolds Number External Flows

Douglas L. Dwoyer

APRIL 1980

NASA

NASA Technical Paper 1655

Velocity-Split Navier-Stokes Solution Procedure for Incompressible High Reynolds Number External Flows

Douglas L. Dwoyer
Langley Research Center
Hampton, Virginia

National Aeronautics
and Space Administration

**Scientific and Technical
Information Office**

1980

SUMMARY

A method for solving the Navier-Stokes equations based on splitting the velocity vector into its rotational and irrotational parts has recently been applied successfully to internal flow computations. In this paper, the applicability of the method to external flows is examined by studying several model problems. The model problems are those of laminar and turbulent incompressible flow past a semi-infinite flat plate and laminar incompressible flow past a finite flat plate. For these problems, the procedure accurately reproduces the known solutions and is computationally very efficient even at high Reynolds numbers. Computational aspects of the method are discussed along with the possibility of using the procedure to retrofit a viscous capability into existing potential-flow codes.

INTRODUCTION

In recent years techniques for predicting the viscous flows over airfoils have been developed based on the numerical solution of the Navier-Stokes equations (ref. 1). Although such solutions are useful, their speed of convergence is limited by the speed at which the basic numerical scheme can solve the Euler equations. For example, the method of Beam and Warming (ref. 2) solves the full Navier-Stokes equations in 20 percent more time than the same method takes for the Euler equations. An alternative to the direct solution of the Navier-Stokes equations has recently been proposed by Dodge (ref. 3). According to Dodge, the velocity vector is split into its rotational and irrotational components. This split, coupled with an appropriate identification of the pressure, leads to a modified potential equation for the pressure field and a set of transport equations for the rotational component of the velocity. The potential equation and the transport equations are then solved separately, with their coupling accounted for by iteration. The advantage of this method is that all the well-developed technology for solving the potential equation can be used for solving the pressure-field equation. Such a procedure can thus take advantage of the more rapid solution procedures available for the potential equation compared with the Euler equations.

The technique proposed by Dodge has primarily been applied to internal flows (ref. 3). Consequently, an investigation was started to examine the suitability of the procedure for solving external flows with the goal of calculating viscous flow fields about airfoils.

In the current investigation, several aspects of the procedure used by Dodge are investigated. The first question addressed in the current work is whether the procedure accurately recovers known solutions to the Navier-Stokes equations for laminar flows. Secondly, the suitability of the procedure for predicting turbulent flows is examined. Both of these questions are studied by calculating high Reynolds number flow over a semi-infinite flat plate. It is recognized that the semi-infinite plate problem can be handled well by conven-

tional boundary-layer theory. The final phase of the study is therefore involved with solution of a problem that cannot be treated by the usual boundary-layer methods. The problem of interest in this report is the detailed prediction of the laminar flow in the vicinity of the trailing edge of a finite flat plate. Computed results for all three problems studied are compared with known solutions.

Use of trade names or names of manufacturers in this report does not constitute an official endorsement of such products or manufacturers, either expressed or implied, by the National Aeronautics and Space Administration.

SYMBOLS

A_x	constant in x-direction coordinate stretch
A_y	constant in y-direction coordinate stretch
B	coordinate scale factor (see eq. (13))
C	constant in coordinate transformation
C_f	skin-friction coefficient
F	reciprocal of mesh interval in x-direction
G	reciprocal of mesh interval in y-direction
I	number of iterations to convergence
M	maximum mesh increment counter in x-direction
N	maximum mesh increment counter in y-direction
P	pressure coefficient with triple-deck scaling
p	pressure
R	Reynolds number based on free-stream conditions
R_x	Reynolds number based on x
r	residual of continuity equation
U	x-component of total velocity vector with triple-deck scaling
u	x-component of total velocity vector
u_r	x-component of rotational part of velocity vector
V	total velocity

v_r	rotational part of velocity
v	y-component of total velocity vector
v_r	y-component of rotational part of velocity vector
x	longitudinal coordinate
x_1	longitudinal coordinate when mesh increment counter is 1
$\tilde{x}$	stretched x-coordinate
$\tilde{x}_1$	stretched x-coordinate when mesh increment counter is 1
y	normal coordinate
$\tilde{y}$	stretched y-coordinate
α	grid stretching parameter
β, β_B	constants in free-stream potential function
δ	boundary-layer thickness
ε	eddy viscosity
η	normal coordinate in Görtler transformation
λ_1	ratio of local wall shear to local Blasius theory wall shear
ξ	longitudinal coordinate in Görtler transformation
ρ	density
Φ	irrotational velocity potential
ϕ	perturbation irrotational velocity potential
ϕ_∞	unperturbed irrotational velocity potential
χ	longitudinal coordinate with triple-deck scaling

Subscripts:

m	mesh increment counter in x-direction
n	mesh increment counter in y-direction
te	trailing-edge location
x, ξ	differentiation in x-direction

y,η differentiation in y-direction

∞ free-stream conditions

Superscripts:

I global iteration counter

' turbulent fluctuating quantity

$\rightarrow$ vector quantity

PROBLEM FORMULATION

Governing Equations

In the present work the governing equations are the incompressible Navier-Stokes equations. These equations may be written as

$$\vec{\nabla} \cdot \vec{V} = 0 \tag{1}$$

$$(\vec{V} \cdot \vec{\nabla})\vec{V} = -\vec{\nabla}p - R^{-1}\vec{\nabla} \times \vec{\nabla} \times \vec{V} \tag{2}$$

where lengths have been nondimensionalized by a reference length L, velocity by the free-stream velocity V_∞, and pressure by $\frac{1}{2}\rho V_\infty^2$. The velocity vector $\vec{V}$ is split into rotational and irrotational components according to the relation

$$\vec{V} = \vec{\nabla}\Phi + \vec{V}_r \tag{3}$$

Further, the pressure is defined, as discussed in reference 3, in terms of the irrotational component as

$$p = C - \frac{1}{2}\vec{\nabla}\Phi \cdot \vec{\nabla}\Phi \tag{4}$$

where C is an arbitrary constant. Substitution of equations (3) and (4) into equations (1) and (2) gives

$$\nabla^2\Phi = -\vec{\nabla} \cdot \vec{V}_r$$

$$(\vec{v}_r \cdot \vec{\nabla})\vec{\nabla}\Phi + \left[(\vec{\nabla}\Phi + \vec{v}_r) \cdot \vec{\nabla}\right]\vec{v}_r = -R^{-1}\vec{\nabla} \times \vec{\nabla} \times \vec{v}_r$$

For turbulent flow in two dimensions, these equations can be time averaged and expanded to give

$$\Phi_{xx} + \Phi_{yy} = -(u_r)_x - (v_r)_y \tag{5}$$

$$u_r\Phi_{xx} + v_r\Phi_{xy} + (\Phi_x + u_r)(u_r)_x + (\Phi_y + v_r)(u_r)_y = R^{-1}\left[(u_r)_{yy} + (\nabla^2\Phi)_x\right] - (u'v')_y \tag{6}$$

$$u_r\Phi_{xy} + v_r\Phi_{yy} + (\Phi_x + u_r)(v_r)_x + (\Phi_y + v_r)(v_r)_y = R^{-1}\left[(v_r)_{yy} + (\nabla^2\Phi)_y\right] \tag{7}$$

The only component of the Reynolds stress tensor retained is the $u'v'$ usually retained in boundary-layer theory. Streamwise diffusion is neglected.

In the current work, with streamwise diffusion neglected, equations (6) and (7) are parabolic. However, equation (5), the pressure equation, still retains its elliptic character. Note that this system of equations has more generality than the usual boundary-layer equations; it admits a normal pressure gradient in the viscous layer. It is also more general than the usual "parabolized" Navier-Stokes equations; it does not require a split of the pressure into a known marching direction pressure gradient and a viscous perturbation pressure field. (See, e.g., ref. 4.)

Boundary Conditions

As indicated in the Introduction, the problem of interest in the current investigation is laminar and turbulent flow over semi-infinite and finite flat plates. The computational domain considered and the associated boundary conditions on the primitive variables are shown in figure 1. The leading edge of the plate was excluded from the computational domain. Therefore, techniques for dealing with the leading-edge singularity did not have to be considered (ref. 5). This subject is left to a future investigation. The inflow boundary of the computational domain is taken sufficiently far downstream of the plate leading edge that effects of the plate leading-edge singularity have vanished and the flow is well described by the Blasius boundary-layer profile with an undisturbed external flow (which is not precisely accurate, but is accurate to $R_x^{-1/2}$ for large enough distances from the leading edge).

The boundary conditions on Φ and $\vec{V}_r$ are obtained from the boundary conditions on the primitive variables as follows:

Wall boundary

$$\left.\begin{aligned} u_r &= -\Phi_x \\ v_r &= \Phi_y = 0 \end{aligned}\right\} \qquad (y = 0, \quad x \leq x_{te})$$

Wake centerline boundary

$$\left.\begin{aligned} (u_r)_y &= v_r = 0 \\ \Phi_y &= 0 \end{aligned}\right\} \qquad (y = 0, \quad x > x_{te})$$

Since the flow is irrotational outside the boundary layer, the rotational component of velocity must vanish outside the boundary layer.

$y \to \infty$ boundary

$$\left.\begin{aligned} u_r &= v_r = 0 \\ \Phi &= \phi_\infty \end{aligned}\right\} \qquad (y \to \infty, \quad 1 \leq x \leq \infty)$$

where ϕ_∞ represents some as yet unspecified potential function.

$x \to \infty$ boundary

$$\Phi = \phi_\infty \qquad (x \to \infty, \quad 0 \leq y \leq \infty)$$

No boundary conditions are required on u_r and v_r as $x \to \infty$, since the transport equations governing their evolution are parabolic.

The boundary conditions along the line $x = 1$ pose a particular problem for the present method, since the splitting of the known total velocity vector into rotational and irrotational components is not unique. The initial choice made in the present investigation was the Blasius velocity profile and zero longitudinal pressure gradient.

Inflow boundary condition

$$u_r = u - (\phi_\infty)_x \qquad (x = 1, \quad 0 \leq y \leq \infty) \qquad (8a)$$

$$v_r = v - (\phi_\infty)_y \qquad (x = 1, \quad 0 \leqq y \leqq \infty) \qquad (8b)$$

$$\Phi_x = 0 \qquad (x = 1, \quad 0 \leqq y \leqq \infty) \qquad (8c)$$

However, computational results forced modification to these conditions which are discussed in some detail in a subsequent section.

Turbulence Model

The Reynolds stress term in equation (6) is modeled with the usual eddy viscosity assumption; that is,

$$-u'v' = \varepsilon \frac{\partial u}{\partial y}$$

Substitution of the x-component of equation (3) into the preceding equation gives

$$-u'v' = \varepsilon(u_r)_y + \varepsilon\phi_{xy} \qquad (9)$$

Substitution of equation (9) into equation (6) leaves the specification of ε to close the system of governing equations. In the present work, a two-layer eddy viscosity formulation is used, as discussed by Cebeci and Smith (ref. 6). In the inner region the formulation is based on Prandtl's mixing-length model along with the Van Driest damping factor. In the outer region, Clauser's velocity defect model is used. No normal intermittency is used.

SOLUTION OF GOVERNING EQUATIONS

General Solution Strategy

In the present work, the governing equations, equations (5) to (7), are solved with a finite-difference procedure. The general strategy of the solution, as proposed in reference 3, is to solve equation (5) separately from equations (6) and (7), and to account for their coupling iteratively. This procedure allows the use of the technology available for solving the potential equation, thus treating the pressure-field solution as an elliptic problem, while still solving the viscous portion of the flow field with a marching calculation.

In practice, the solution procedure is started by first determining the inviscid pressure field by specifying an initial potential function which satisfies equation (5) with the right-hand side set to zero. Once the Φ field is established, the u_r and v_r fields are established by solving equations (6)

and (7) with a marching solution initiated by the assumed profile at $x = 1$. All the required Φ derivatives in equations (6) and (7) are known functions and are calculated from the solution of equation (5). Once the u_r and v_r fields are found, $\vec{\nabla} \cdot \vec{v}_r$ can be calculated and treated as a known source term for the solution of equation (5). This process is continued until the continuity equation is satisfied throughout the field to some required degree of tolerance; that is,

$$|r^I| = |(\nabla^2\Phi)^I + (\vec{\nabla} \cdot \vec{v}_r)^I| < \text{Tolerance} \qquad (1 < x < \infty, \quad 0 \leq y < \infty) \tag{10}$$

where the superscript I refers to iteration number.

Transformation of Momentum Equations

Examination of equations (6) and (7) reveals that they need only be solved in regions where the velocity has a nonzero rotational part; that is, in the viscous layer. In most situations the viscous layer has the characteristic that its thickness increases in the streamwise direction. For this reason, the boundary-layer equations are usually transformed into a coordinate system in which the height of the viscous layer is approximately constant. For comparative purposes, a similarity transformation is introduced in the current investigation by introducing Görtler scaling on the normal coordinate.

The x-coordinate is now alined with the free-stream direction and the following new independent variables are introduced:

$$\xi = x \tag{11}$$

$$\eta = \left[B(\xi)\right]^{-1} y \tag{12}$$

where

$$B(\xi) = 1 \tag{13a}$$

if the normal coordinate is not transformed, and

$$B(\xi) = (2\xi)^{1/2} \tag{13b}$$

if the normal coordinate is transformed by Gortler scaling. In these new variables, equations (6) and (7) become, after substitution of equation (9),

$$B^2(u_r\Phi_{xx} + v_r\Phi_{xy}) + B^2(u_r + \Phi_x)(u_r)_\xi + \left[B(v_r + \Phi_y) - \bar{B}\eta(u_r + \Phi_x)\right](u_r)_\eta$$

$$= R^{-1}\left\{\left[(1 + \varepsilon)(u_r)_\eta\right]_\eta + B^2(\nabla^2\Phi)_x - B^2(\varepsilon\Phi_{xy})_y\right\} \tag{14}$$

$$B^2(u_r\Phi_{xy} + v_r\Phi_{yy}) + B^2(u_r + \Phi_x)(v_r)_\xi + \left[B(v_r + \Phi_y) - \bar{B}\eta(u_r + \Phi_x)\right](v_r)_\eta$$

$$= R^{-1}\left[(v_r)_{\eta\eta} + B^2(\nabla^2\Phi)_y\right] \tag{15}$$

where $\bar{B} = (B - 1)/(2\xi - 1)$.

Numerical Method

Solutions to the system of equations (5), (14), and (15), with their associated boundary conditions, are obtained with finite-difference methods. Since equation (5) and equations (14) and (15) are of different types, the numerical techniques used in their solution differ. Equation (5) is solved by the successive line overrelaxation method (SLOR) discussed in reference 7; equations (14) and (15) are solved by using an implicit marching technique.

Consider first the finite-difference mesh used in the solution. In all cases, the equations are solved on nonuniform meshes. Stretched Cartesian coordinates are used in the solution of the potential equation (eq. (5)) for all cases, and are used in the solution of the viscous equations (eqs. (14) and (15)) when $B = 1$. The general mesh notation is indicated in figure 2. The nonuniform Cartesian mesh is obtained by coordinate transformations of the form

$$x = \frac{A_x\tilde{x}}{\sqrt{1 - \tilde{x}^2}} + x_o \tag{16}$$

$$y = \frac{A_y\tilde{y}}{\sqrt{1 - \tilde{y}^2}} \tag{17}$$

where $x_o = 0$ for the semi-infinite flat-plate case and $x_o = x_{te}$ for the finite flat-plate case. The actual computations are carried out in the $\tilde{x},\tilde{y}$ plane with a uniform mesh. The step sizes in the $\tilde{x}$- and $\tilde{y}$-directions are

$$\Delta\tilde{x} = \frac{C}{M - 1}$$

$$\Delta\tilde{y} = \frac{1}{N - 1}$$

where $C = 1$ for the semi-infinite plate, $C = 1 + \dfrac{x_1}{\sqrt{A_x^2 + \tilde{x}_1^2}}$ for the finite plate, and $\tilde{x}_1 = \tilde{x}_{te} - 1$.

When $B = (2\xi)^{1/2}$, different meshes are used in the solution of equation (5) and equations (14) and (15). For this case, the stretched Cartesian grid is used for equation (5), whereas the η-coordinate in equations (14) and (15) is stretched using the Roberts transformation (ref. 8). This transformation can be written as

$$\eta = \eta_{max}\left\{1 - \left[(\alpha + 1)(\alpha^{1-N} - 1)\right]\left[(\alpha - 1)(\alpha^{1-N} + 1)\right]^{-1}\right\}$$

where α is a stretching parameter. Equation (16) is still used to stretch the x-coordinate.

Now consider the solution to equation (5). In the present work, equation (5) is solved for a disturbance potential by writing

$$\nabla^2\Phi = \nabla^2(\phi_\infty + \phi) = -\vec{\nabla} \cdot \vec{v}_r$$

and, since ϕ_∞ is chosen such that

$$\nabla^2\phi_\infty = 0$$

then

$$\nabla^2\phi = -\vec{\nabla} \cdot \vec{v}_r \tag{18}$$

Now F_m and G_n are defined as

$$F_m = (\Delta\tilde{x})^{-1} \frac{d\tilde{x}}{dx}$$

$$G_n = (\Delta\tilde{y})^{-1} \frac{d\tilde{y}}{dy}$$

With this notation, equation (18) is discretized according to

$$\phi_{xx} = \left[(\phi_{m+1,n} - \phi_{m,n}) F_{m+(1/2)} - (\phi_{m,n} - \phi_{m-1,n}) F_{m-(1/2)} \right] F_m \qquad (19a)$$

$$\phi_{yy} = \left[(\phi_{m,n+1} - \phi_{m,n}) G_{n+(1/2)} - (\phi_{m,n} - \phi_{m,n-1}) G_{n-(1/2)} \right] G_n \qquad (19b)$$

The boundary conditions are discretized according to

$$\phi_{m,1} = \phi_{m,3} \qquad (2 \leq m \leq M - 1)$$

$$\phi_{1,n} = \phi_{2,n} \qquad (1 \leq n \leq N)$$

$$\phi_{m,N} = 0 \qquad (1 \leq m \leq M - 1)$$

$$\phi_{M,n} = 0 \qquad (2 \leq n \leq N)$$

The discretized representation of equation (18) is solved by the SLOR procedure with y as the implicit direction and with the procedure sweeping from $n = 2$ to $n = N - 1$ on each iteration cycle. The most recent values of ϕ are used whenever possible. The Thomas algorithm is used to solve the set of implicit tridiagonal equations along each line where m is constant. If $r_{m,n}$ is defined as

$$\left| (\nabla^2\phi)_{m,n} + (\vec{\nabla} \cdot \vec{v}_r)_{m,n} \right|$$

then convergence is achieved when

$$r_{m,n} \leqq \frac{1}{2}(\Delta\tilde{x}^2 + \Delta\tilde{y}^2) \qquad (2 \leqq m \leqq M - 1, \quad 2 \leqq n \leqq N - 1)$$

Now consider the solution of the rotational-velocity-component momentum transport equations, equations (14) and (15). These equations are parabolic in the ξ-direction and hence are solved by downstream marching from an initial profile located at $\xi = 1$. If g denotes either u_r or v_r, then equations (14) and (15) are discretized according to

$$(g_x)_{m,n} = \frac{1}{2}(3g_{m,n} - 4g_{m-1,n} + g_{m-2,n})F_m \tag{20a}$$

$$(g_y)_{m,n} = \frac{1}{2}(g_{m,n+1} - g_{m,n-1})G_n \tag{20b}$$

$$(g_{yy})_{m,n} = \left[(g_{m,n+1} - g_{m,n})G_{n+(1/2)} - (g_{m,n} - g_{m,n-1})G_{n-(1/2)}\right]G_n \tag{20c}$$

If these equations were substituted directly into equations (14) and (15), a set of $N - 2$ simultaneous nonlinear algrebraic equations would result along the mth column. Thus, before discretization, equations (14) and (15) are quasi-linearized. When f is either a u_r or v_r derivative, then

$$(fg)_{m,n} = (\tilde{f}g)_{m,n} + (f\tilde{g})_{m,n} - (\tilde{f}\tilde{g})_{m,n}$$

where the tildes mean guessed values. Substitution of these relations into equations (14) and (15) yields a set of $2(N - 2)$ simultaneous linear algebraic relations. The equation set can be completed by using the boundary conditions

$$(u_r)_{m,1} = -(\Phi_x)_{m,1}$$

$$(v_r)_{m,1} = -(\Phi_y)_{m,1}$$

$$(u_r)_{m,N} = 0$$

$$(v_r)_{m,N} = 0$$

This system of equations is then solved by the Gaussian elimination for a 2×2 block tridiagonal matrix.

Quasi-linearization of the viscous term requires special attention in turbulent cases. The nonlinear viscous term in equation (14) can be written as

$$\frac{\partial}{\partial \eta}\left[(1 + \varepsilon)\frac{\partial u_r}{\partial \eta}\right] = \frac{\partial}{\partial \eta}\left\{\left[1 + a(\delta) + b\frac{\partial u_r}{\partial \eta}\right]\frac{\partial u_r}{\partial \eta}\right\}$$

where $a(\delta)$ is a function of boundary-layer thickness δ and b is a constant (ref. 9). The quasi-linear form is then

$$\frac{\partial}{\partial \eta}\left\{\left[1 + a(\tilde{\delta}) + 2b\frac{\partial \tilde{u}_r}{\partial \eta}\right]\frac{\partial u_r}{\partial \eta} - b\left(\frac{\partial \tilde{u}_r}{\partial \eta}\right)^2\right\}$$

As can be seen, this form does not properly quasi-linearize the term $a(\delta)\dfrac{\partial u_r}{\partial \eta}$, since δ is a function of the local solution. With this form, quadratic convergence is obtained on the column iterations for the laminar cases, whereas for the turbulent cases a 20-percent decrease in computer time over Picard iteration is achieved.

In the solution of equation (5), $\vec{\nabla} \cdot \vec{v}_r$ is treated as a known quantity at each mesh point. In the solution of equations (14) and (15), however, Φ and all its required derivatives are treated as known. The quantity $\vec{\nabla} \cdot \vec{v}_r$ is numerically evaluated for each rotational-velocity-component calculation by using equations (20a) and (20b). The quantities Φ_{xx} and Φ_{yy} are calculated after each solution for Φ by using equations (19) along with known values of $\phi_{\infty_{xx}}$ and $\phi_{\infty_{yy}}$. In addition, the following relationships are used to obtain other required derivatives of ϕ.

$$(\Phi_x)_{m,n} = \frac{1}{2}(\phi_{m+1,n} - \phi_{m-1,n})F_m + \left(\phi_{\infty_x}\right)_{m,n}$$

$$(\Phi_y)_{m,n} = \frac{1}{2}(\phi_{m,n+1} - \phi_{m,n-1})G_n + \left(\phi_{\infty y}\right)_{m,n}$$

$$(\Phi_{xy})_{m,n} = \frac{1}{4}(\phi_{m+1,n+1} - \phi_{m-1,n+1} + \phi_{m-1,n-1} - \phi_{m+1,n-1})F_m G_n + \left(\phi_{\infty xy}\right)_{m,n}$$

$$(\nabla^2\Phi)_{m,n} = (\phi_{xx})_{m,n} + (\phi_{yy})_{m,n}$$

$$\left[(\nabla^2\Phi)_x\right]_{m,n} = \frac{1}{2}\left[(\nabla^2\phi)_{m+1,n} - (\nabla^2\phi)_{m-1,n}\right]F_m$$

$$\left[(\nabla^2\Phi)_y\right]_{m,n} = \frac{1}{2}\left[(\nabla^2\phi)_{m,n+1} - (\nabla^2\phi)_{m,n-1}\right]G_n$$

Since these quantities are required only on interior mesh points, special formulas on the boundaries are not required.

It should be noted that in the actual programming of the scheme, provision was made for resolving the rotational component of velocity on a finer mesh than the irrotational component. When $B = 1$, this was done by breaking up the $\tilde{x}$- and/or $\tilde{y}$-increments in the computational plane into the desired integer number of subincrements. When this provision was made, the derivatives of Φ required in the solution of equations (14) and (15) were linearly interpolated onto the finer grid.

When Görtler variables are used for solution of equations (14) and (15), linear interpolation on both Φ and $\vec{\nabla} \cdot \vec{V}_r$ is used.

RESULTS AND DISCUSSION

As discussed previously, three test cases were chosen for computation with the split Navier-Stokes formulation. These cases are the laminar and turbulent semi-infinite flat plate and the finite flat plate. The computer results for these test cases are discussed separately in the following sections.

Laminar Semi-Infinite Flat Plate

It is well known that a singularity exists in the pressure and vorticity at the leading edge of a flat plate (ref. 5). Rather than deal with this problem in the current investigation, all solutions were initiated a sufficient distance downstream of the leading edge such that the effects of this

singularity were negligible. According to reference 5, at a Reynolds number based on distance from the leading edge R_x of 10^4 the boundary layer is well described by the Blasius velocity profile. For the current computations, the free-stream conditions were such that $R_x = 10^4$ for $x = 1$. The initial computations were started at $x = 1$ with the Blasius velocity profile. This profile was generated in the program itself by numerical solutions of the appropriate nonlinear ordinary differential equations (ref. 10).

In order to initiate the calculation, a choice had to be made for ϕ_∞, the basic potential function. The most obvious choice to make was

$$\phi_\infty = x + \text{Constant} \tag{21}$$

since this represents the undisturbed inviscid flow about a flat plate. This choice led to immediate difficulties in equation (8b) since $(\phi_\infty)_y$ is zero everywhere. Use of the Blasius-predicted v in equation (8b) would then lead to nonzero values of v as $y \to \infty$, which is physically incorrect. For this reason, v was arbitrarily set to zero along the initial profile when this form was chosen for ϕ_∞.

A second possible choice for ϕ_∞ is that for flow about the displacement body presented by the plate boundary layer to the inviscid flow. It is well known that the flat-plate displacement body is a parabola which has infinite thickness as $x \to \infty$. In fact, the velocity potential is infinite as $y \to \infty$ for such bodies, whereas the boundary conditions and equation (21) indicate a finite value for the potential function as $y \to \infty$. One way to alleviate this difficulty is to choose the potential function for flow about the Blasius displacement-body parabola for ϕ_∞; that is,

$$\phi_\infty = x + \frac{\beta R^{-1/2}}{\sqrt{2}} \frac{y}{\left[x + (x^2 + y^2)^{1/2}\right]^{1/2}}$$

where $\beta = \beta_B = 1.72078765$ for the Blasius displacement body (ref. 11). Note that when $\beta = 0$ the uniform-stream potential function is recovered. The preceding potential function predicts nonzero values of $(\phi_\infty)_y$ along the initial data line; that is,

$$(\phi_\infty)_y = \frac{\beta R^{-1/2}}{2\sqrt{2}} \frac{\left[x + (x^2 + y^2)^{1/2}\right]^{1/2}}{(x^2 + y^2)^{1/2}}$$

Thus, the normal-velocity profile on the inflow boundary is assumed to have the following form:

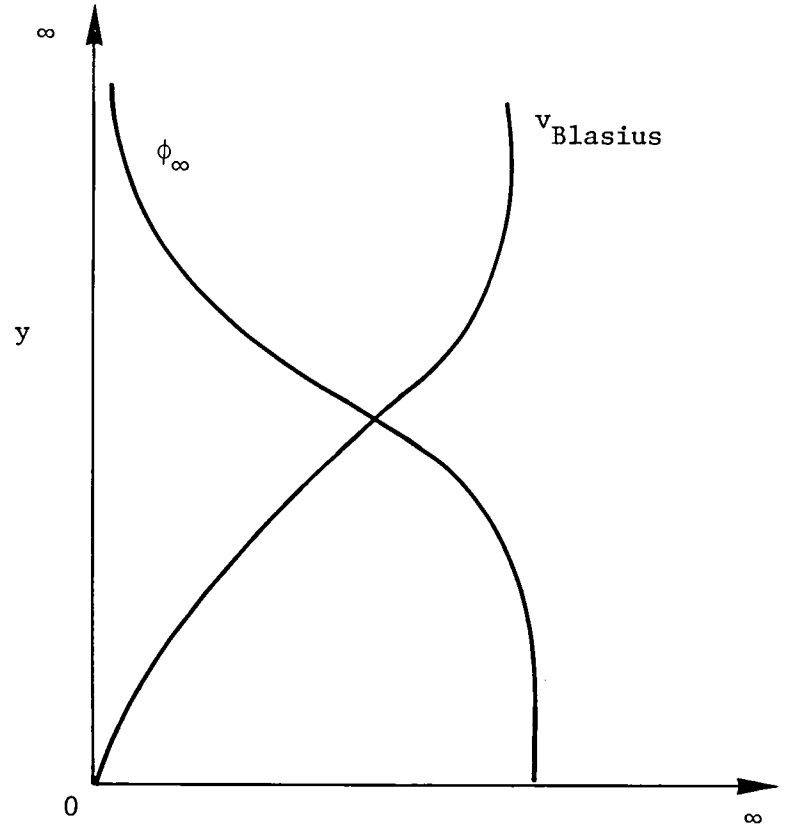

Normal-velocity components

$$v_r = v_{Blasius} - (\phi_\infty)_y \qquad v_{Blasius} \leqq (\phi_\infty)_y$$

$$v_r = -(\phi_\infty)_y \qquad v_{Blasius} > (\phi_\infty)_y$$

Also, since $(\phi_\infty)_y \neq 0$ along $y = 0$, the surface boundary condition becomes

$$v_r = -(\phi_\infty)_y \qquad (y = 0, \quad 1 \leqq x < \infty)$$

Calculations were made for the semi-infinite plate using these two free-stream potential functions on a mesh with 41 points in the x-direction and 58 points in the y-direction, and with $A_x = 20$ and $A_y = 0.22$. For the case where $\beta = \beta_B$, the calculation was stopped when the convergence criterion was satisfied, a total of 44 global iterations (i.e., iterations between eq. (5) and eqs. (14) and (15)). Convergence was extremely slow for the $\beta = 0$ case, however, and the calculations were arbitrarily stopped after 200 iterations with $|\vec{\nabla} \cdot \vec{v}|_{max} = 6.48 \times 10^{-4}$ and the wall shear converged

to four decimal places of accuracy. The distribution of λ_1, the ratio of predicted wall shear to the local Blasius value, along the plate is presented in figure 3 for these cases. As can be seen, the predicted wall shear immediately departs from the Blasius value in the vicinity of $x = 1$ in both solutions. This is attributed to the arbitrary split of the initial velocity distribution into its rotational and irrotational parts. For the case with $\beta = \beta_B$, the Blasius wall shear is quickly recovered further down the plate, whereas the case with $\beta = 0$ never recovers the Blasius solution. This behavior is attributed to the fact that the solution obtained with $\beta = \beta_B$ accounts for the interaction, however weak, between the boundary layer and inviscid flow. The choice of $\beta = 0$ coupled with the boundary condition as $y \to \infty$ ignores this interaction and forces the potential function to vanish as $y \to \infty$. This leads to serious errors, as can be seen in figure 4, in the prediction of the normal-velocity component all the way down to the wall. The conclusion drawn from these calculations was that for interaction calculations involving infinite bodies, the proper choice of boundary conditions at $y \to \infty$ is crucial. No further calculations were made with $\beta = 0$ for the semi-infinite plate.

After establishing the ability of the split equations to accurately reproduce the Blasius solution with coincident meshes for both the pressure (i.e., ϕ) and viscous (i.e., $\vec{V}_r$) solutions, calculations were performed with increasingly coarsened (in the y-direction) pressure meshes while holding the viscous mesh constant. This was accomplished by holding A_y the same on both grids and successively halving the number of points in the y-direction for the pressure calculation. The resulting pressure grid points all coincided with viscous grid points with an integral number of viscous grid points between. Three successive halvings of the number of pressure-mesh points were done over the 41 × 58 mesh. The results of these calculations are presented in table 1 in terms of the percent error in friction drag relative to the Blasius value over the interval $1 \leq x \leq 90.12$, along with the number of iterations to convergence and computer time required. All runs were converged to the truncation error of the pressure mesh. Little accuracy is lost by the coarsening of the pressure mesh, and there is a substantial savings in computer time. The convergence histories of these calculations are presented in figure 5. Coarsening of the pressure mesh is shown to accelerate the overall convergence rate.

To further assess the potential of the velocity-split formulation, additional calculations were carried out with entirely independent meshes for the pressure and viscous calculations by choosing $B = (2\xi)^{1/2}$. This allowed the number of viscous mesh points in the boundary layer to be held constant at about 40 points over the entire length of the plate. In this case, the viscous grid was again held fixed and A_y was varied. Results of these calculations are presented in table 2. In this table, the ratio of the pressure-mesh increment to the viscous mesh increment at the wall is used as a measure of the grid coarsening. It should be noted that in the solutions for mesh ratios of 32.90 and 65.79 ($A_y = 3.52$ and 7.04) the global iteration had to be underrelaxed in order to achieve convergence. The reason for the deterioration of the solution accuracy on the coarser pressure grids is obvious from figure 6. In this figure, the distribution of $\vec{\nabla} \cdot \vec{V}_r$ across the boundary layer is plotted along with the location of both the viscous and pressure-mesh points. As can be seen, when the pressure grid is coarsened to the point that it can no longer resolve the distribution of $\vec{\nabla} \cdot \vec{V}_r$, serious deterioration in accuracy

occurs. Also presented in table 2 are the error in the local wall shear at $x = 33.33$ and the number of pressure-mesh points in the boundary layer. These data can be interpreted as a first-order estimate of the number of pressure mesh points that are required in the boundary layer to give adequate resolution. From table 2 it can be seen that between 5 and 10 pressure-mesh points are required within the boundary layer to accurately predict the local wall shear.

Turbulent Semi-Infinite Flat Plate

The semi-infinite plate was also run for the turbulent case. In this case, the value of R_x was 1.0×10^6 at $x = 1.0$. The solution was started from the Blasius solution at $x = 1.0$, and instantaneous transition was arbitrarily introduced at $x = 2.44$ $(m = 4)$. For this case the value of β was the laminar value since the exact potential-flow solution about the turbulent displacement body was not known.

The distribution of skin friction along the plate is compared in figure 7 with the Prandtl-Schlichting formula for a smooth flat plate (ref. 10). For the cases shown the grid was defined by the following parameters:

Viscous	Inviscid
$M = 41$	$M = 41$
$N = 54$	$N = 61$
$\alpha = 2048$	$A_y = 0.2, 0.3, 0.4$
$\eta_\varepsilon = 0.08$	$A_x = 20$
$A_x = 20$	

The solutions for the three values of A_y cannot be differentiated on the scale of figure 7. For values of $A_y > 0.4$, however, the solutions diverged while values of $A_y < 0.2$ left too few points outside the boundary layer on the inviscid mesh, and hence were not run. The three cases of $A_y = 0.2$, 0.3, and 0.4 took 17, 15, and 54 global iterations requiring 35, 30, and 102 seconds, respectively, on the Control Data CYBER 175 computer to achieve convergence.

The turbulent case thus appears somewhat more sensitive to the resolution of the boundary layer by the pressure calculation than the laminar case. For the case of $A_y = 0.4$, the first pressure grid point off the wall corresponds to $y/\delta = 0.37$ at $x = 2.44$, the first turbulent profile. For the turbulent case, resolution coarser than this leads to divergent solutions rather than inaccurate solutions as in the laminar case. On the other hand, these results show that the pressure grid does not have to resolve the details of the turbu-

lent boundary layer near the wall in order to produce accurate results, provided the viscous mesh is fine enough.

In view of the results for the laminar case, the apparent accuracy of the turbulent calculations is surprising since the basic potential function does not properly account for the decay of the normal component of velocity as $y \to \infty$. It should first be noted, however, that the predicted solution in figure 7 does begin to depart from the data curve fit at the higher values of R_x and examination of the normal-velocity profiles in this vicinity does show some small negative values near the wall. Secondly, the values predicted by any finite-difference program of this type depend upon the transition history and turbulence model employed. Thus, for this case an exact solution is not available for comparison, as in the laminar case. Hence, a direct quantitative error estimate is not possible. In addition, it can be seen from figure 7 that the predicted values of skin friction are in error in the laminar region. This error is attributed to the upstream influence of the transition region through the pressure calculation.

It should finally be noted that for turbulent calculations the Newton iteration in the viscous marching-column solution did not converge quadratically. This is in agreement with the results of reference 9.

Finite Flat Plate

The third problem chosen for solution in the current investigation is the laminar finite flat plate for $R = 5 \times 10^4$. In this problem, a singularity exists at the trailing edge of the plate due to the discontinuous boundary condition. Calculations were made with the present method using coincident pressure and viscous meshes with $\beta = 0$. Results of these calculations are shown in figures 8 to 10. In these figures, the following triple-deck scaled quantities are presented:

$$\chi = \frac{\lambda^{5/4}(x - x_{te})}{\varepsilon^3 x_{te}}$$

$$U = \frac{u}{\varepsilon \lambda^{1/4}}$$

$$P = \frac{p - p_\infty}{\frac{1}{2} \varepsilon^2 \lambda^{1/2}}$$

$$\varepsilon = R^{-1/8} \qquad (\lambda = 0.33206)$$

These results are compared with the triple-deck theory solutions of Melnik and Chow (ref. 12) and Jobe and Burggraf (ref. 13). Figure 8 presents the wall/centerline pressure distribution in the vicinity of the trailing edge, figure 9 the wall shear, and figure 10 the wake centerline velocity distribution. Agreement between the present calculations and triple-deck theory is excellent. The better agreement between the present results and those of reference 13 is attributed to the fact that the results of reference 12 were calculated on a much finer grid than that used in either the current calculations or those of reference 13. Additional calculations were made with the pressure solution obtained on every second and fourth viscous mesh point with no plottable difference in the results. The calculations required 75 seconds of CYBER 175 time for the coincident mesh case, whereas the two coarser grid calculations required 50 and 39 seconds, respectively.

CONCLUDING REMARKS

It is concluded from the current investigation that the split-velocity Navier-Stokes formulation can be used to obtain accurate solutions to the Navier-Stokes equations for finite and semi-infinite flat plates. Results of the pressure-mesh coarsening studies carried out in this investigation also indicate that the method can be used to retrofit a viscous capability into existing potential-flow codes. In order to retrofit such a capability, however, care must be taken to adequately resolve the viscous layer with the pressure grid. Since existing potential-flow computer programs have computational grids selected to resolve purely inviscid phenomena, only in special cases can the retrofit be made without altering the grid. For the commonly used numerical schemes in modern potential-flow programs, the introduction of a known function on the right-hand side of the potential equation poses no difficulty.

For the problems studied in the current investigation, the computational efficiency of the method appears unaffected by Reynolds number. The reason is that in any given calculation the bulk of the computational effort (about 80 percent) is in the viscous marching calculation. In this portion of the calculation, the effect of Reynolds number is accounted for by scaling the viscous grid. Hence, the total computation time for a given viscous marching sweep is unaffected by Reynolds number. Finer resolution of the viscous region by the pressure grid at higher Reynolds number does slow this portion of the calculation down but has little effect on the overall computation time. For this reason, the method appears promising for calculating steady, high Reynolds number, external flows.

Langley Research Center
National Aeronautics and Space Administration
Hampton, VA 23665
March 18, 1980

REFERENCES

1. Steger, Joseph L.: Implicit Finite-Difference Simulation of Flow About Arbitrary Two-Dimensional Geometries. AIAA J., vol. 16, no. 7, July 1978, pp. 679-686.

2. Beam, Richard M.; and Warming, R. F.: An Implicit Factored Scheme for the Compressible Navier-Stokes Equations. AIAA J., vol. 16, no. 4, Apr. 1978, pp. 393-402.

3. Dodge, P. R.: Numerical Method for 2D and 3D Viscous Flows. AIAA J., vol. 15, no. 7, July 1977, pp. 961-965.

4. Briley, W. Roger: Numerical Method for Predicting Three-Dimensional Steady Viscous Flow in Ducts. J. Comput. Phys., vol. 14, no. 1, Jan. 1974, pp. 8-28.

5. Davis, R. T.: Numerical Solution of the Navier-Stokes Equations for Symmetric Laminar Incompressible Flow Past a Parabola. J. Fluid Mech., vol. 51, pt. 3, Feb. 1972, pp. 417-433.

6. Cebeci, Tuncer; and Smith, A. M. O.: Analysis of Turbulent Boundary Layers. Academic Press, Inc., 1974.

7. Roache, Patrick J.: Computational Fluid Dynamics. Hermosa Publ., c.1972.

8. Roberts, Glyn O.: Computational Meshes for Boundary Layer Problems. Proceedings of the Second International Conference on Numerical Methods in Fluid Dynamics. Volume 8 of Lecture Notes in Physics, Maurice Holt, ed., Springer-Verlag, 1971, pp. 171-177.

9. Carter, James E.: Inverse Boundary-Layer Theory and Comparison With Experiment. NASA TP-1208, 1978.

10. Schlichting, Hermann (J. Kestin, transl.): Boundary-Layer Theory. Sixth ed. McGraw-Hill Book Co., Inc., c.1968.

11. Stewartson, K.: On Asymptotic Expansions in the Theory of Boundary Layers. J. Math. & Phys., vol. XXXVI, no. 3, Oct. 1957, pp. 173-191.

12. Melnik, R. E.; and Chow, R.: Asymptotic Theory of Two-Dimensional Trailing-Edge Flows. Aerodynamic Analyses Requiring Advanced Computers - Part I, NASA SP-347, 1975, pp. 177-249.

13. Jobe, C. E.; and Burggraf, O. R.: The Numerical Solution of the Asymptotic Equations of Trailing Edge Flow. Proc. Roy. Soc. London, ser. A, vol. 340, no. 1620, Sept. 3, 1974, pp. 91-111.

TABLE 1.- EFFECT OF PRESSURE-MESH COARSENING ON

OVERALL SOLUTION ACCURACY FOR RELATED MESHES

Number of y-points (pressure)	Percent error in friction drag	I	CYBER 175 time, sec
58	-0.50	45	47
30	-1.40	25	20
16	3.70	12	8
9	3.73	9	6

TABLE 2.- EFFECT OF PRESSURE-MESH COARSENING ON

SOLUTION ACCURACY FOR INDEPENDENT MESHES

Wall mesh ratio	Percent error in friction drag	x = 33.33	
		Number of y-points in boundary layer (pressure)	λ_1
2.06	-0.49	46	0.998
4.11	-.70	32	.996
8.23	-.16	19	.998
16.45	2.46	10	1.029
32.90	13.4	5	1.142
65.79	23.0	3	1.327

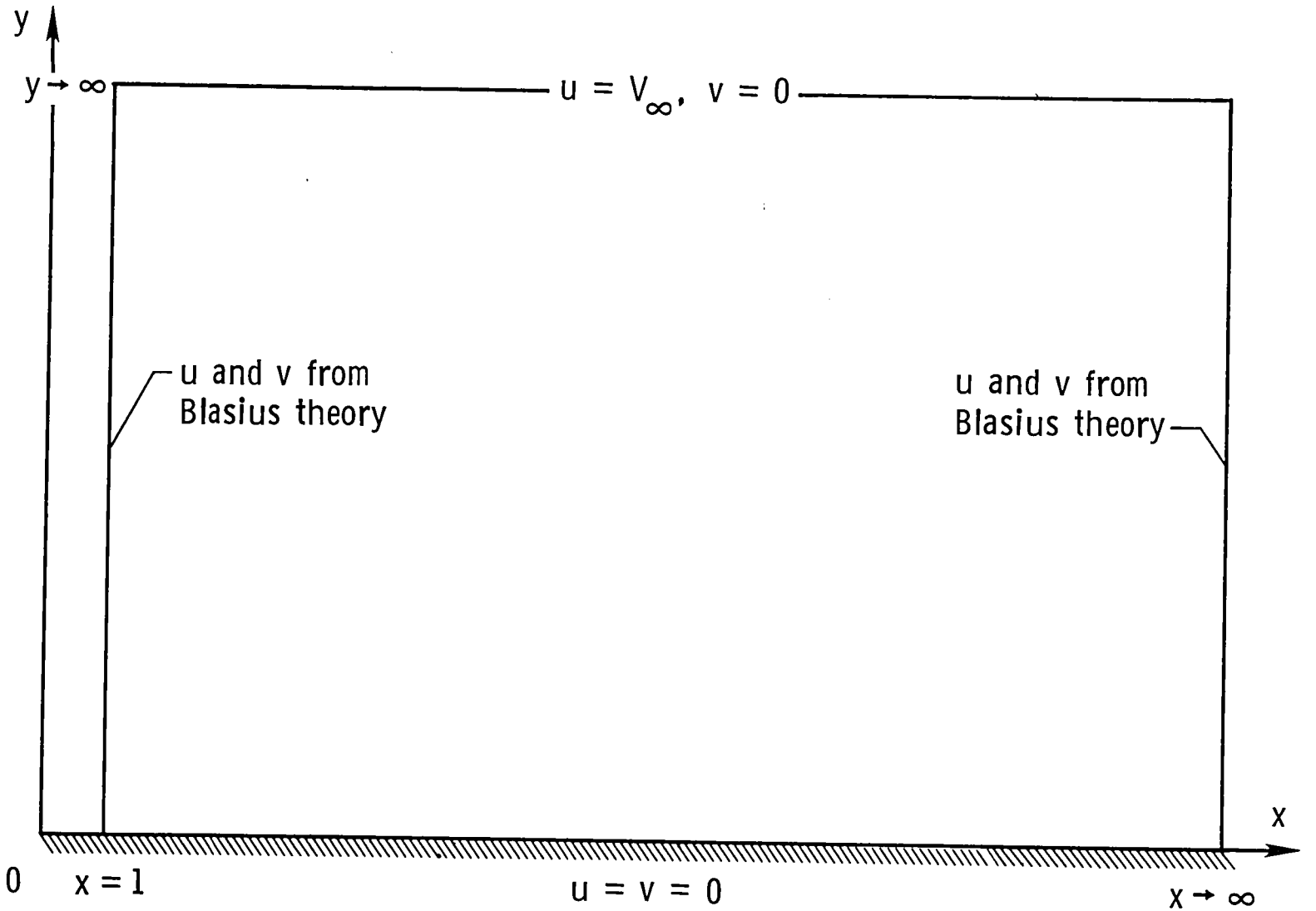

(a) Semi-infinite flat plate.

Figure 1.- Coordinate system and boundary conditions for test problem.

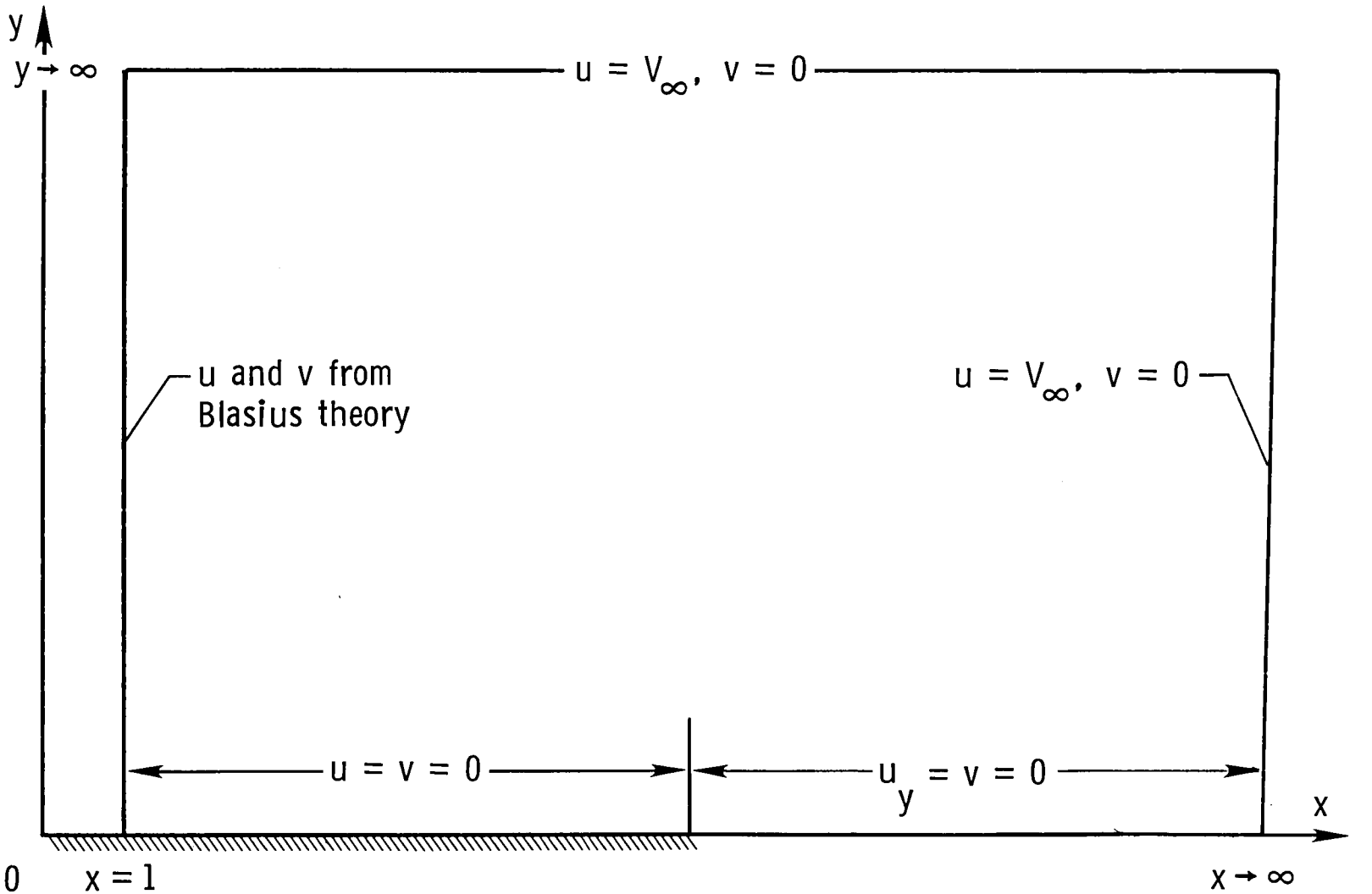

(b) Finite flat plate.

Figure 1.- Concluded.

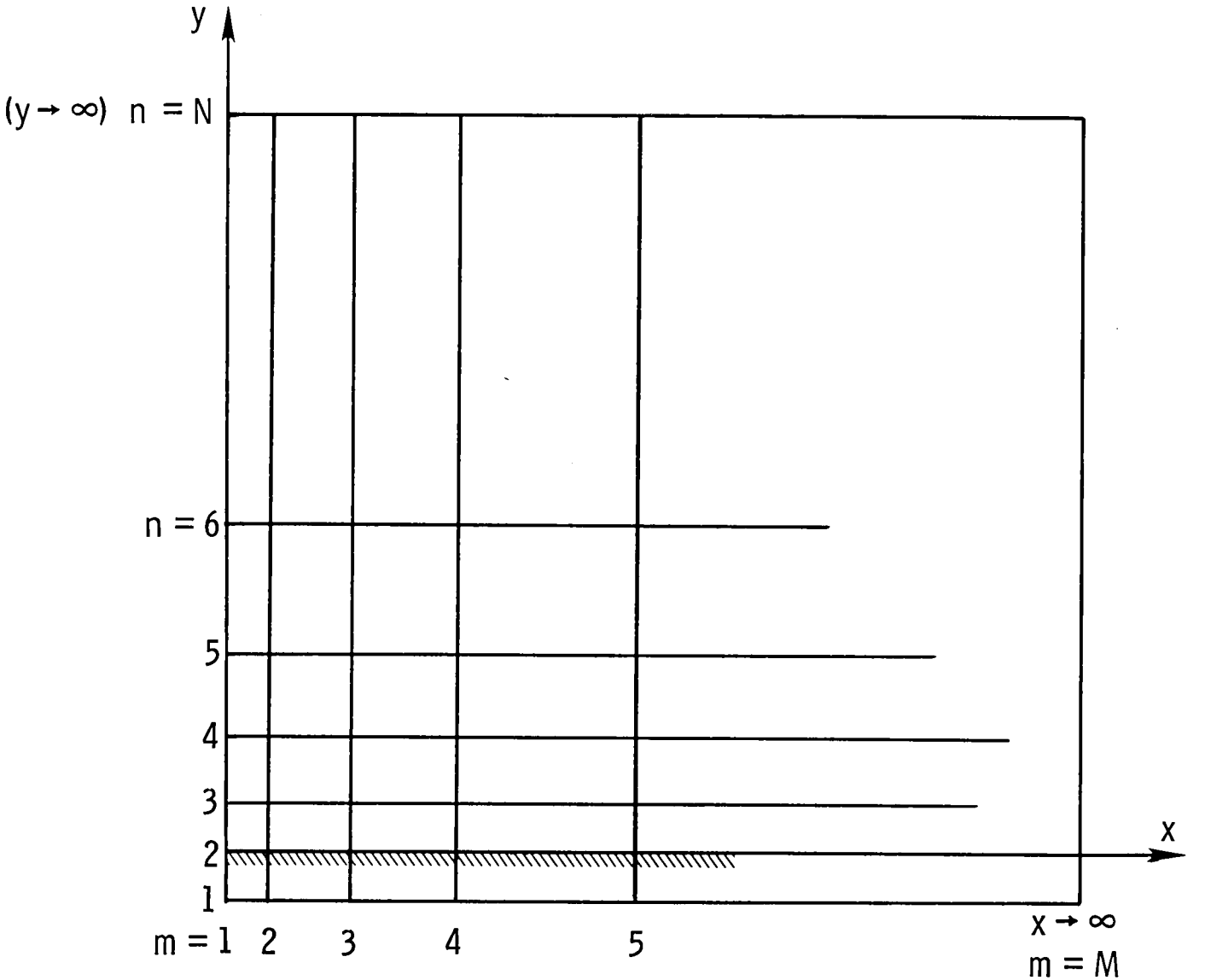

Figure 2.- Finite-difference grid for semi-infinite and finite flat-plate problems.

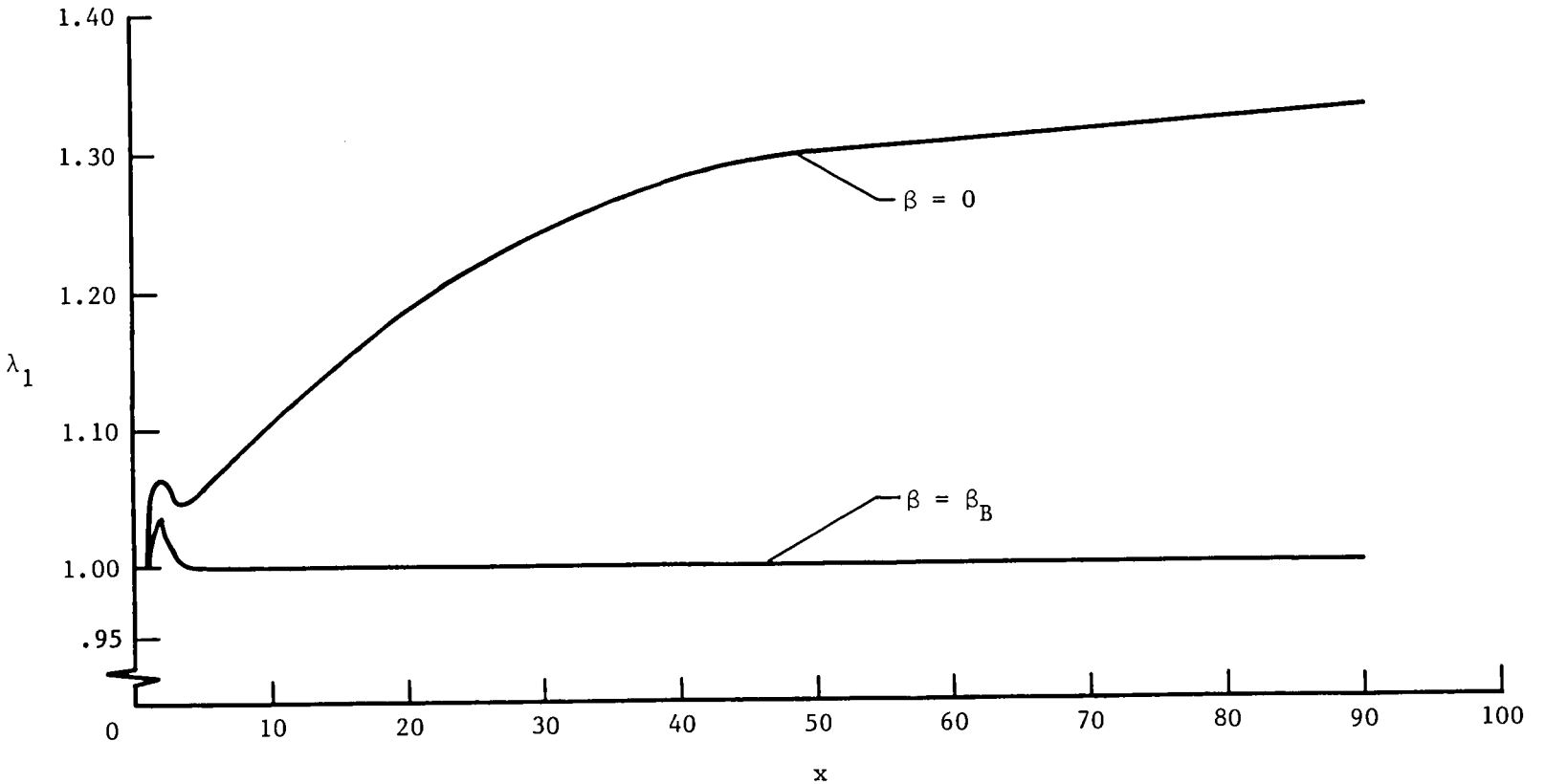

Figure 3.- Effect of free-stream potential function on normalized wall-shear distribution.

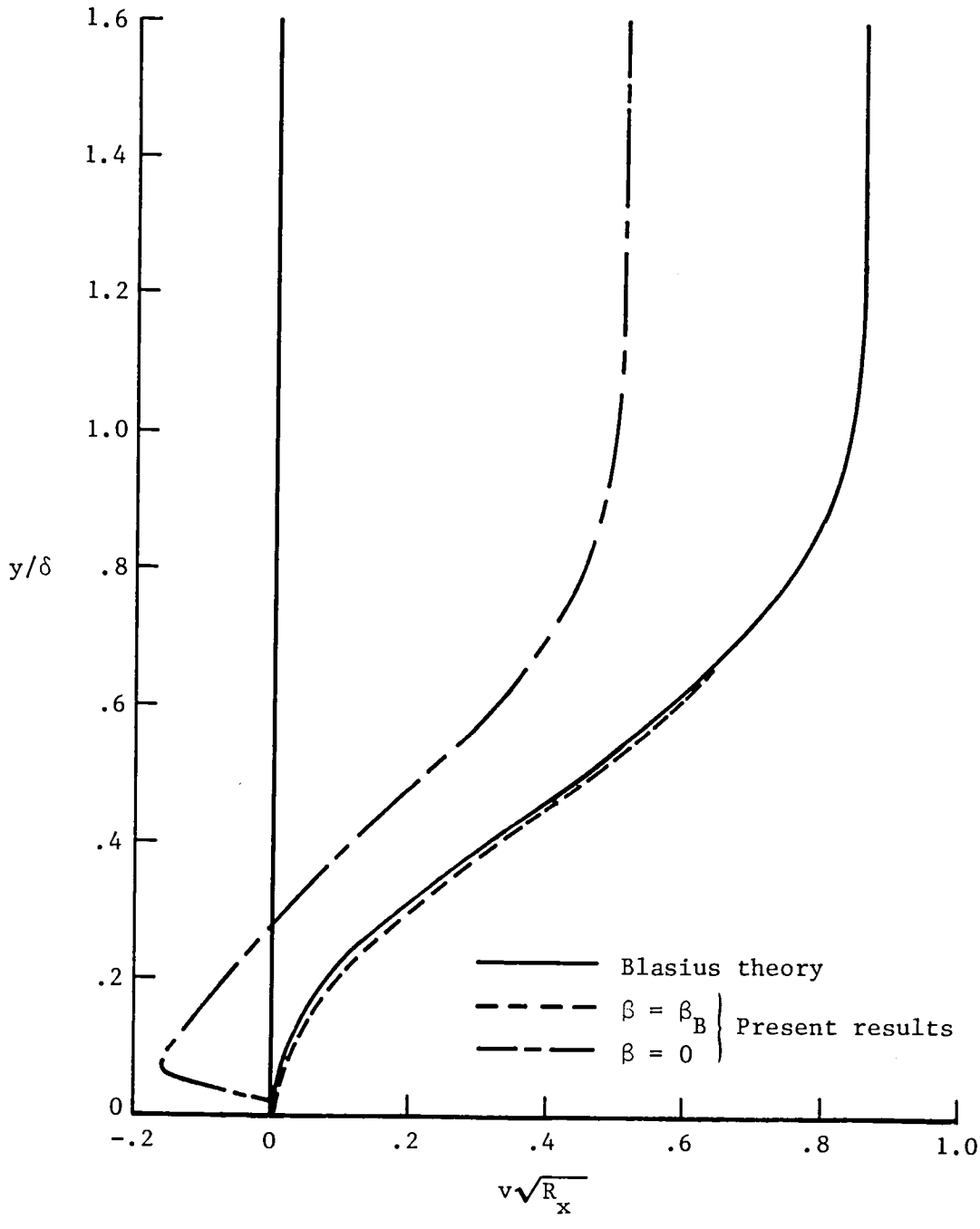

Figure 4.- Effect of free-stream potential function on boundary-layer normal-velocity distribution.

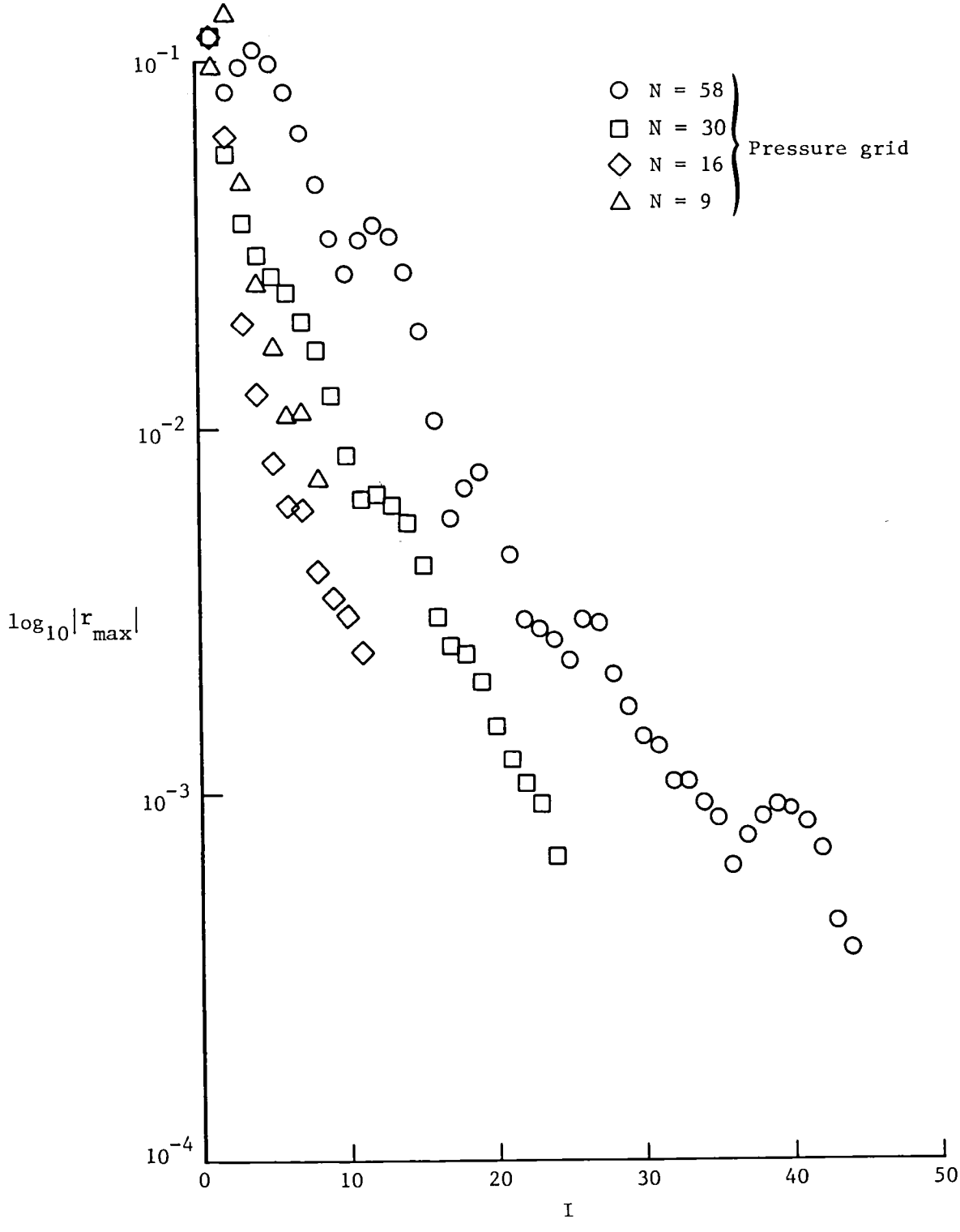

Figure 5.- Effect of pressure-mesh coarsening on convergence of global iteration.

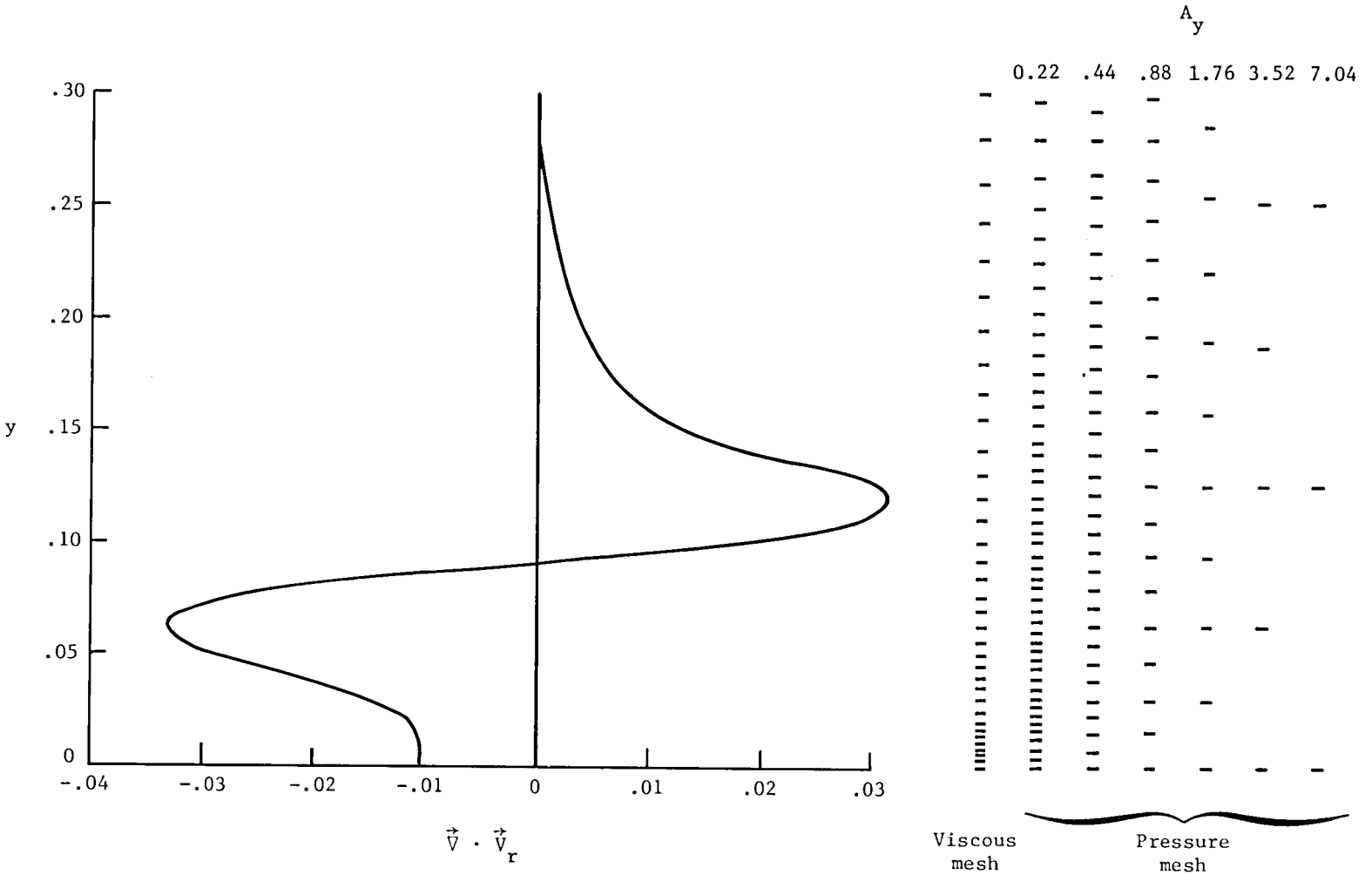

Figure 6.- Typical distribution of $\vec{V} \cdot \vec{V}_r$ through a boundary layer compared with location of pressure-mesh points.

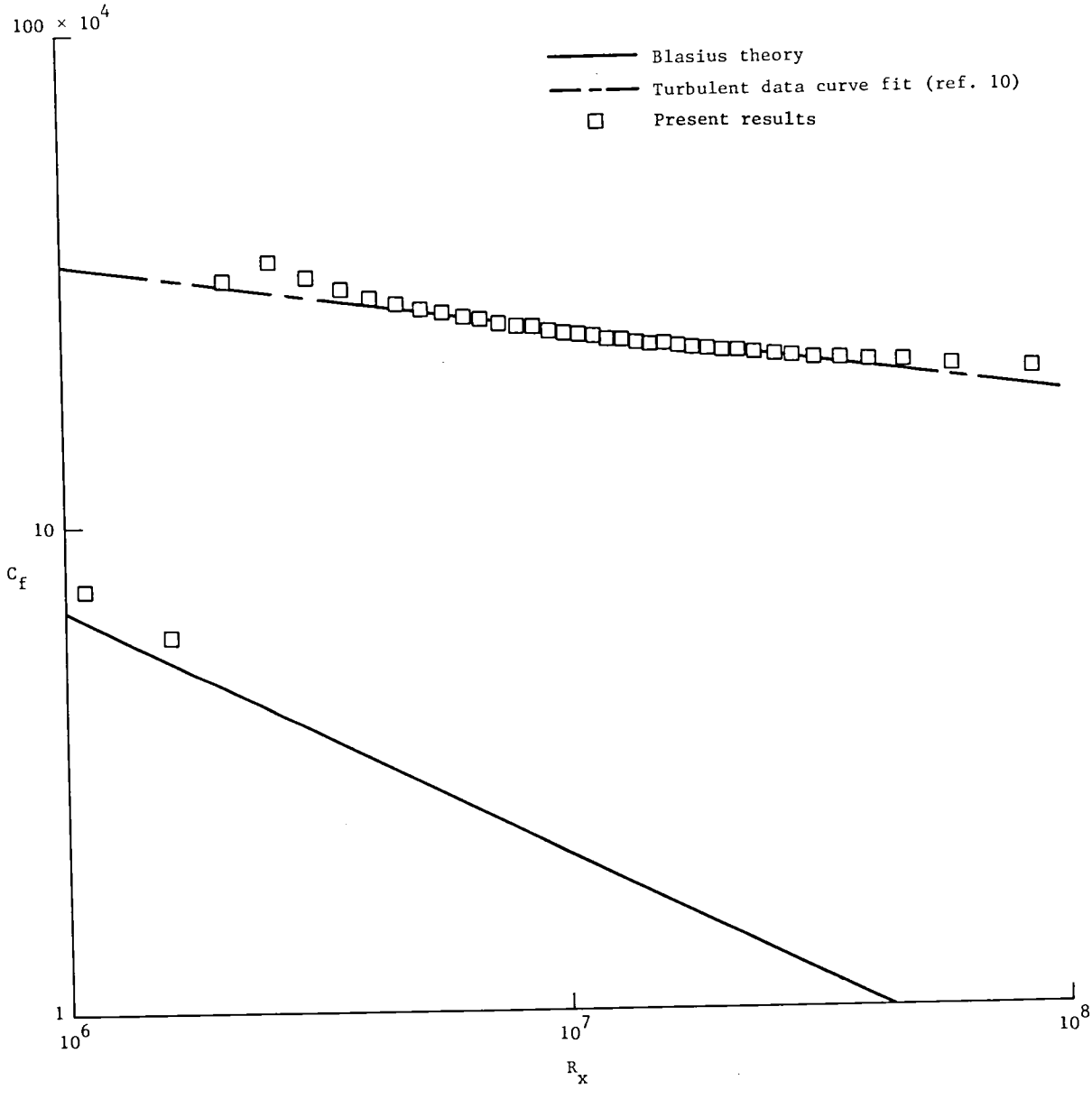

Figure 7.- Skin-friction distribution along a flat plate in turbulent flow.

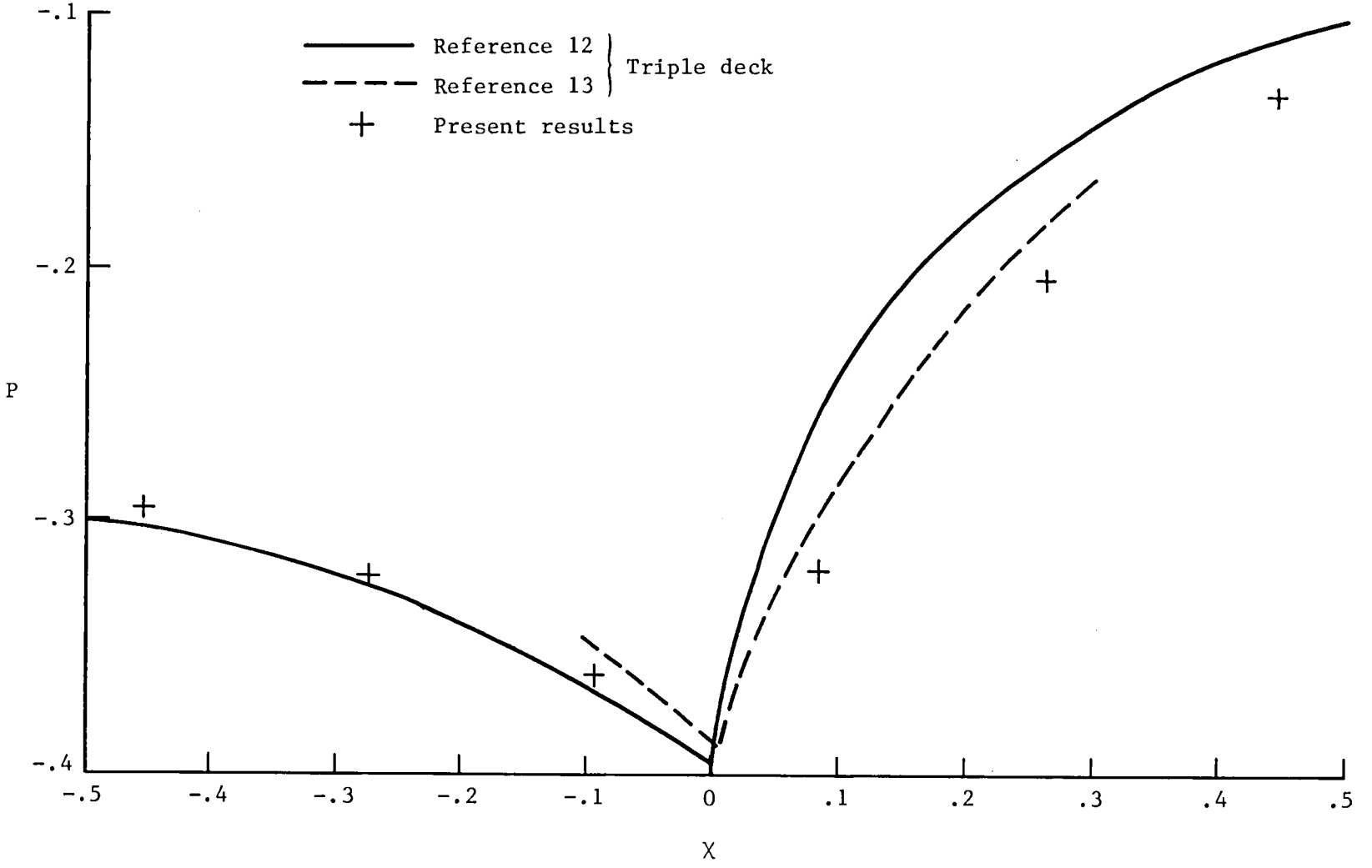

Figure 8.- Pressure distribution near trailing edge of a flat plate (R_{te} = 50 000).

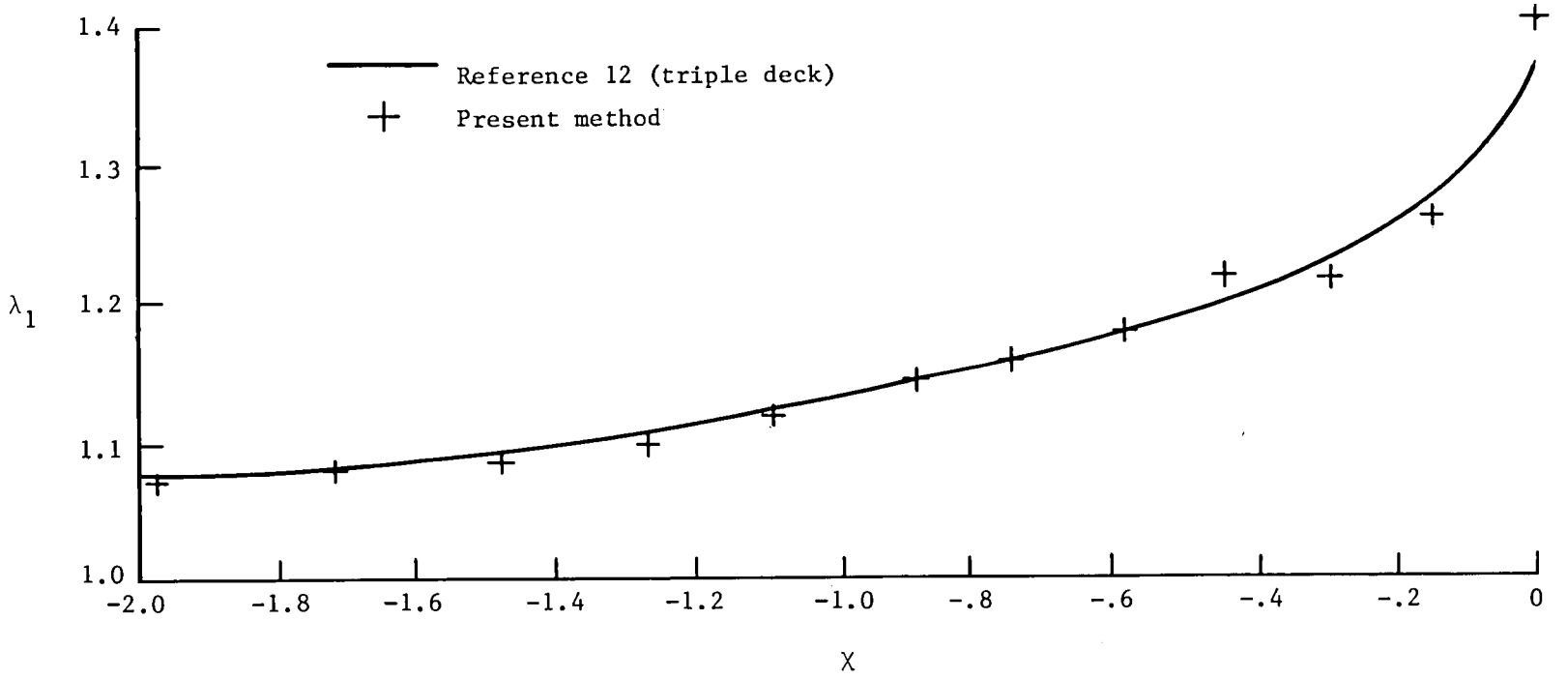

Figure 9.- Wall-shear distribution near trailing edge of a flat plate (R_{te} = 50 000).

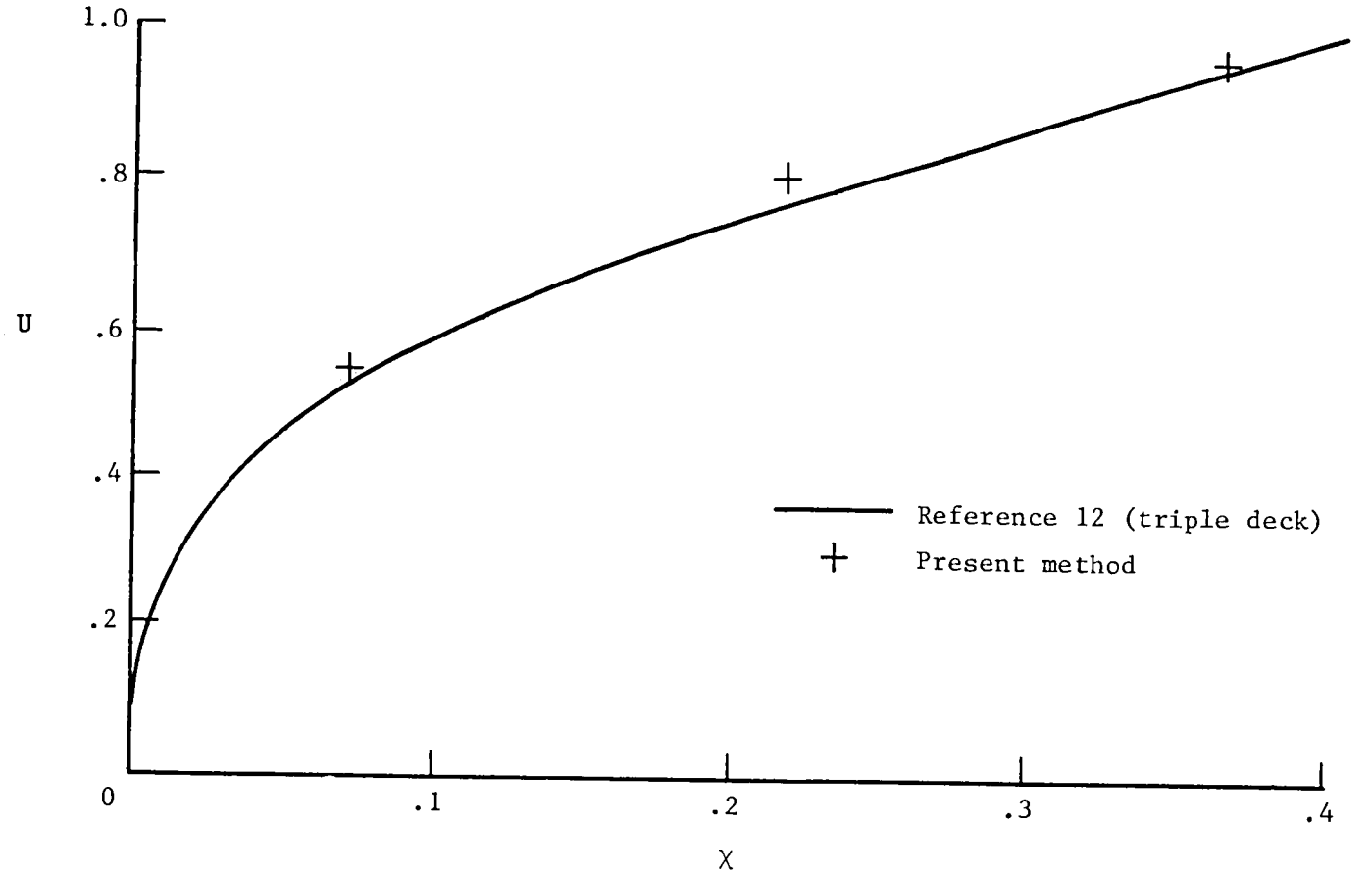

Figure 10.- Wake centerline velocity distribution near trailing edge of a flat plate (R_{te} = 50 000).

1. Report No.	2. Government Accession No.	3. Recipient's Catalog No.
NASA TP-1655		

4. Title and Subtitle	5. Report Date
VELOCITY-SPLIT NAVIER-STOKES SOLUTION PROCEDURE FOR INCOMPRESSIBLE HIGH REYNOLDS NUMBER EXTERNAL FLOWS	April 1980
	6. Performing Organization Code

7. Author(s)	8. Performing Organization Report No.
Douglas L. Dwoyer	L-13343
	10. Work Unit No. 505-31-13-10

9. Performing Organization Name and Address	11. Contract or Grant No.
NASA Langley Research Center Hampton, VA 23665	
	13. Type of Report and Period Covered Technical Paper
12. Sponsoring Agency Name and Address National Aeronautics and Space Administration Washington, DC 20546	14. Sponsoring Agency Code

15. Supplementary Notes

16. Abstract

A method for solving the Navier-Stokes equations based on splitting the velocity vector into its rotational and irrotational parts has recently been applied successfully to internal flow computations. In this paper, the applicability of the method to external flows is examined by studying several model problems. The model problems are those of laminar and turbulent incompressible flow past a semi-infinite flat plate and laminar incompressible flow past a finite flat plate. For these problems, the procedure accurately reproduces the known solutions and is computationally very efficient even at high Reynolds numbers. Computational aspects of the method are discussed along with the possibility of using the procedure to retrofit a viscous capability into existing potential-flow codes.

17. Key Words (Suggested by Author(s))	18. Distribution Statement
Navier-Stokes Viscous flow Computational fluid dynamics	Unclassified - Unlimited Subject Category 34

19. Security Classif. (of this report)	20. Security Classif. (of this page)	21. No. of Pages	22. Price*
Unclassified	Unclassified	33	$4.50

* For sale by the National Technical Information Service, Springfield, Virginia 22161

NASA-Langley, 1980

National Aeronautics and Space Administration

Washington, D.C.
20546

Official Business
Penalty for Private Use, $300

THIRD-CLASS BULK RATE

Postage and Fees Paid
National Aeronautics and
Space Administration
NASA-451

NASA

POSTMASTER: If Undeliverable (Section 158 Postal Manual) Do Not Return